HHS Public Access

Author manuscript

Science. Author manuscript; available in PMC 2016 December 01.

Published in final edited form as:

Science. 2016 March 4; 351(6277): aad3680. doi:10.1126/science.aad3680.

Activation of PKA leads to mesenchymal-to-epithelial transition and loss of tumor-initiating ability

Diwakar R. Pattabiraman[1], **Brian Bierie**[1], **Katharina Isabelle Kober**[1], **Prathapan Thiru**[1], **Jordan Krall**[1], **Christina Zill**[1], **Ferenc Reinhardt**[1], **Wai Leong Tam**[1,4,5], and **Robert A. Weinberg**[1,2,3,*]

[1]Whitehead Institute for Biomedical Research, Cambridge, Massachusetts, USA

[2]Department of Biology, Massachusetts Institute of Technology, Cambridge, Massachusetts, USA

[3]Ludwig MIT Center for Molecular Oncology, Cambridge, Massachusetts, USA

[4]Genome Institute of Singapore, 60 Biopolis Street, Singapore

[5]Cancer Science Institute of Singapore, 14 Medical Drive, Singapore

Abstract

The epithelial-to-mesenchymal transition (EMT) enables carcinoma cells to acquire malignancy-associated traits and properties of tumor-initiating cells (TICs). TICs have emerged in recent years as important targets for cancer therapy owing to their ability to drive clinical relapse and enable metastasis. Here we propose a strategy to eliminate mesenchymal TICs by inducing their conversion to more epithelial counterparts that have lost tumor-initiating ability. We report that increases in intracellular levels of the second messenger, cAMP, and the subsequent activation of protein kinase A (PKA) induce a mesenchymal-to-epithelial transition (MET) in mesenchymal human mammary epithelial cells. Activation of PKA triggers PHF2-mediated epigenetic reprogramming of TICs, promoting their differentiation that leads to loss of tumor-initiating ability. This study provides proof-of-principle for inducing an MET as differentiation therapy for TICs and uncovers a novel role for PKA in enforcing and maintaining the epithelial state.

One Sentence Summary

We identify a novel role for the activation of PKA and downstream epigenetic reprogramming that results in the differentiation of tumor-initiating cells in aggressive breast cancers.

Introduction

Tumor-initiating cells (TICs), also known as cancer stem cells, are defined operationally by their ability to seed new tumors upon implantation in appropriate hosts. They have emerged in recent years as important targets for cancer therapy owing to their elevated resistance to conventional chemotherapy and their tumor-initiating ability; the latter allowing them to metastasize and drive clinical relapse (1, 2). While their mode of generation and biological

*Correspondence: weinberg@wi.mit.edu (R.A.W.).

Supplementary Figures 1–11, Supplementary Tables 1–4

properties have been explored in a diverse array of cancer types (3), our understanding of the biology of TICs remains superficial. Cytotoxic therapies designed specifically to eliminate TICs might be targeted, for example, to interdict the signaling pathways that are used preferentially or uniquely by these cells (4). At present, however, the nature of such TIC-specific signaling pathways remains to be fully elucidated.

The epithelial-to-mesenchymal transition (EMT) is a cell-biological program that confers mesenchymal traits on both normal and neoplastic epithelial cells (5). In addition, activation of an EMT program enables both classes of cells to acquire stem-like properties (6, 7). Indeed, TICs from several carcinoma types possess distinct mesenchymal attributes, suggesting that they have passed, at least partially, through an EMT (7–9). This association between the EMT program and the TIC state has presented an attractive opportunity for drug development, using agents that preferentially target more mesenchymal carcinoma cells rather than their epithelial counterparts in an effort to eliminate TICs.

At least two approaches might be taken to target mesenchymal TICs. One strategy would be to develop agents that show specific or preferential cytotoxicity toward TICs (1). In this study, we have embraced an alternative strategy that is designed to induce TICs to exit the more mesenchymal tumor-initiating state and enter into an epithelial non-stemlike state. Such induced differentiation should, we reasoned, place cells in a state where they would become more vulnerable to conventional cytotoxic treatments. Accordingly, we screened for agents that could induce a mesenchymal-to-epithelial transition (MET) and thereby uncovered the central role of 3’-5’-cyclic adenosine monophosphate (cAMP) and its downstream target, protein kinase A (PKA), in governing the transition of cells from the mesenchymal to the epithelial state.

cAMP is a second messenger that transmits intracellular signals upon interaction of certain hormones and neurotransmitters with receptors on the plasma membrane (10). cAMP regulates multiple downstream effectors; the first of these to be identified and the most well-studied is protein kinase A (PKA) (11), which plays numerous roles in various cell types and operates in several subcellular locations (11). Being initially assembled as a heterotetrameric holoenzyme, the activity of PKA depends on binding of cAMP to its two regulatory subunits, which leads to the release of active catalytic subunits and the phosphorylation of a diverse array of substrates (12).

In previous work, PKA has been shown, under some conditions, to promote an EMT; PKA was shown to regulate Snail in one study and another study demonstrated that HIF1α could regulate transcription of *PRKACA* under hypoxic conditions (13, 14). On the other hand, PKA signaling has been shown to favor the epithelial state, but the mechanistic understanding of this phenomenon is very limited. One report identified that schwannomas in *Prkar1a* (encoding the PKA regulatory subunit)-null mice exhibited loss of vimentin and gain of cytokeratins and E-cadherin (15), whereas another study revealed inhibition of formation of mesoderm-derived structures in Prkar1a null mice (16). A recent study reported that deletion of the Gαs subunit repressed the activity of PKA, limiting the proliferative potential of epithelial hair follicle stem cells (17). Nevertheless, the connection of PKA

signaling to TICs and the stem-like state is poorly understood and the exploitation of this pathway as a differentiation-based cancer therapy has not been explored.

Results

Identification of agents that induce an MET in mammary epithelial cells

Human breast cancers are characterized by cells exhibiting various degrees of epithelial and mesenchymal properties as revealed by the expression pattern of markers such as cytokeratins and vimentin (Fig S1). Almost 85% of the carcinomas we examined showed varied expression patterns of cytokeratins, indicating that the loss of epithelial properties is a commonly occurring event. Notably, ~10% of the carcinomas we examined exhibited high degrees of intra-tumoral heterogeneity, created in part by the presence of subpopulations of neoplastic cells that exhibit both epithelial and mesenchymal properties. These are reminiscent of cells that have undergone an EMT, resembling TICs that possess a higher tumor-initiating propensity and an increased resistance to chemotherapy (18). To model the behavior of these subpopulations of carcinoma cells from human basal-like breast cancers, we used HMLE immortalized human mammary epithelial cells (19), which display an epithelial morphology, express E-cadherin at adherens junctions and low levels of mesenchymal markers such as vimentin and fibronectin. They also exhibit a $CD44^{lo}/CD24^{hi}$ cell surface marker phenotype that is characteristic of previously reported cells that lack stemlike properties (non-CSCs) (20). We also used their spontaneously arising mesenchymal derivatives, termed NAMEC8 (N8) cells (21). Relative to their HMLE counterparts, N8 cells express mesenchymal markers such as vimentin and fibronectin as well as the EMT-inducing transcription factors Snail and Zeb1 at higher levels, lack expression of E-cadherin and prominent cell junctions, and display a CSC-like $CD44^{hi}/CD24^{lo}$ cell surface marker profile (Fig 1A to C). They also possess a greater propensity to form mammospheres (Fig 1D, E), which is often used as an *in vitro* surrogate assay for the stemness of mammary epithelial cells. They are more efficient at migration through a transwell membrane and invasion through a Matrigel-coated Boyden chamber membrane (Fig 1F and G); both *in vitro* assays represent models of cancer cell invasiveness *in vivo*. N8 cells are also more resistant to treatment with chemotherapeutic drugs such as doxorubicin and paclitaxel (Fig 1H, I), as shown previously (21). Hence, two cell types represent epithelial and mesenchymal derivatives of mammary epithelial cells of common origin that were used to model the two cell states and how they impact tumor initiation and progression.

To search for agents that can induce an MET, we performed a screen to identify compounds that could induce transcription of *CDH1*, which encodes E-cadherin, a key epithelial protein, in N8 cells. As a reporter for the activity of the *CDH1* gene, we constructed a lentiviral vector that expresses a portion of the *CDH1* promoter fused to luciferase (Fig S2A). We performed a screen using a 400-compound library for agents that were able to induce the *CDH1*-driven luciferase expression in N8 cells (Fig S2B). Most striking was the behavior of forskolin (Fsk), an adenylate cyclase activator that induced a 40-fold increase in luciferase activity (Fig S2C). Another adenylate cyclase activator, cholera toxin (CTx), was also able to induce an increase in luciferase activity (Fig S2D), suggesting that activation of adenylate cyclase could induce the acquisition of epithelial properties.

Forskolin or Cholera Toxin and the induction of an MET in mammary epithelial cells

We found that treatment of N8 cells in monolayer culture with either CTx or Fsk for a period of 14 days induced the formation of islands of cells with the characteristic cobblestone morphology of epithelial cells; such cells acquired the expression of E-cadherin at adherens junctions along with a loss of mesenchymal markers such as vimentin (Fig 1A–C). Also, the cell-surface marker expression profile of the N8 cells switched from a stem-like $CD44^{hi}/CD24^{lo}$ to a non-stem $CD44^{lo}/CD24^{hi}$ phenotype following this treatment (20) (Fig 1B). These shifts were accompanied by a 100-fold increase in *CDH1* mRNA levels, as well as 4-, 5- and 7-fold decreases in the mRNAs levels of *Snail*, *Twist1* and *Zeb1* EMT-inducing transcription factors (EMT-TFs) to 25%, 20% and 14%, respectively, of the N8 cells before the transition (Fig S3A and B). Treatment of N8 cells with either CTx or Fsk resulted in a near-complete loss of mammosphere-forming ability (Fig 1D and E), as well as their ability to migrate and invade (Fig 1F and G). There were no significant differences in the rates of proliferation between the N8 cells and their CTx- and Fsk-treated derivatives (Fig S3C). Of additional interest, withdrawal of CTx after 14 days of treatment led to cell populations that continued to reside in an epithelial state for >2 months in culture.

Reversion to an epithelial state, ostensibly similar to that of HMLE cells, rendered the N8 cells 8 times as sensitive to killing by doxorubicin (lowered the median inhibitory concentration (IC_{50}) from 1.39μM to 0.159μM), and 13 times as sensitive to paclitaxel (lowered the IC_{50} from 4.79μM to 0.35μM) (Fig 1H and I). Additionally, the induced MET also resulted in increased sensitivity to a range of chemotherapeutic drugs and inhibitors including methotrexate, HSP90 inhibitors, proteasome inhibitors, and epidermal growth factor receptor-mitogen-activated protein kinase (EGFR/MAPK) pathway inhibitors, as observed when we screened against two small molecule libraries (Selleck Anti-cancer Compound Library and Enzo Kinase Inhibitor Library)(Fig S4). Hence, the induction of an MET rendered the N8 cells more sensitive to a range of drugs and inhibitors, pointing to its utility as a means of overcoming therapeutic resistance. Additionally, it also reinforces the notion that mesenchymal cells are more resistant to a range of cytotoxic agents.

We then performed mRNA sequencing (mRNA-Seq) to compare the global gene expression profiles of the mesenchymal N8 and the reverted N8-CTx cells in order to view the transcriptional changes that occur following the induction of MET. As determined by differential gene expression (Fig 1J, Table S1 and S2) and principal component analyses (Fig S3D), the N8-CTx cells assume a gene expression profile that is almost completely converted to that of the epithelial HMLE cells and significantly differ from the mesenchymal N8 cells (Fig 1J). Gene set enrichment analyses showed that the changes in gene expression from N8 to the N8-CTx cells are highly similar to several previously published EMT/MET gene signatures (22–24) (Fig S3E).

Taken together, these observations demonstrated a genuine transition of the N8 cells from a mesenchymal-like state to a *bona fide* epithelial state, rendering these cells more sensitive to a variety of drugs with potentially important therapeutic implications.

Effects of Forskolin and Cholera Toxin on intracellular cAMP levels and PKA

To confirm that both Fsk and CTx were working through alteration of cAMP levels, we measured the levels of this second messenger in both HMLE and N8 cells using liquid chromatography - mass spectrometry (LC-MS). Treatment with CTx resulted in a 6–8-fold increase in the intracellular levels of cAMP, which could be dampened by exposure to SQ22536, an inhibitor of adenylate cyclase, the enzyme responsible for the formation of cAMP (Fig 2A).

The major downstream targets of cAMP are exchange proteins activated by cAMP (EPAC1/2) (25), cyclic nucleotide gated ion channels which are primarily found in cells of the kidney, heart, testis and central nervous system (26); and the most commonly studied downstream effector, protein kinase A (PKA) (11). To delineate the downstream pathways that are activated in response to increase in cAMP levels, we treated N8 cells with two cAMP analogs – 8-Bromoadenosine-3',5'-cyclic monophosphate (8-Br-cAMP), which is known to preferentially activate PKA (27) or 8-(4-chlorophenylthio)-2'-O-methyladenosine-3',5'-cyclic monophosphate (8-CPT-2Me-cAMP), which is a selective activator of the exchange proteins activated by cAMP (EPAC) (28). As was seen with Fsk/CTx, treatment with 8-Br-cAMP was also able to induce an MET in N8 cells, whereas 8-CPT-2Me-cAMP treatment had no effect on their mesenchymal properties (Fig 2B). This allowed us to conclude that PKA, rather than the cAMP-activated exchange proteins, was more likely to play a central role in the MET process.

Knockdown of the catalytic subunit of PKA using two different shRNAs (Fig S5A) abrogated the CTx-induced MET process in N8 cells, as demonstrated by their inability to develop a clear epithelial morphology, acquire junctional E-cadherin, and to shed mesenchymal markers such as fibronectin (Fig 2C, D). Moreover, treatment of these PKA-knockdown cells with CTx failed to induce an effective transition from the $CD44^{hi}/CD24^{lo}$ stem-like state to the $CD44^{lo}/CD24^{hi}$ non-stem-like state, which was otherwise observable in the absence of PKA knockdown (Fig 2E). These results further reinforced the important role of PKA in the MET process.

We proceeded to test whether PKA activity, independent of cAMP, was sufficient to induce an MET. Thus, we ectopically expressed a doxycycline-inducible constitutively active, cAMP-independent mutant form of PKA (caPKA) (29) in N8 cells and found that it was capable of inducing a reversion to the epithelial state in 7–10 days (Fig 2F). Hence, it appears as though PKA is both necessary and sufficient to induce an MET in the N8 cells.

We tested the role of CTx/Fsk in inducing an epithelial state in other cell systems to assess the generality of our observations. Removing CTx from the standard culture medium of MCF10A immortalized human mammary epithelial cells (30), caused them to acquire mesenchymal properties, lose cell-cell adherens junctions, lose their characteristic cobblestone morphology, gain a $CD44^{hi}/CD24^{lo}$ cell surface marker profile. They also lost E-cadherin expression and exhibited an increase in expression of *Zeb1*, *Vimentin* and *Fibronectin* (Fig S6A–E). Re-addition of CTx or forced expression of the constitutively active PKA mutant (caPKA) led to the re-acquisition of epithelial features (Fig S6A–E). Moreover, the MCF10A cells that lost epithelial properties upon CTx withdrawal were 4

times as resistant to treatment with doxorubicin, extending our observations made in N8 cells that the mesenchymal variants were more resistant to conventional chemotherapeutic agents (S6F).

We then proceeded to test the role of CTx/Fsk in a series of other cell lines. MCF7-Ras human breast cancer cells (31) can be induced to undergo an EMT through the ectopic expression of EMT-inducing transcription factors, such as Slug. Co-treatment of the cells undergoing an EMT with CTx led to a 48-hour delay in the acquisition of mesenchymal morphology and $CD44^{hi}$ cell-surface marker expression (Fig S7A). Similarly, the ability of HMLE-Ras cells to undergo an EMT upon ectopic expression of Zeb1 was also hampered upon co-treatment with CTx (Fig S7B). PANC1 pancreatic adenocarcinoma cells undergo an EMT upon treatment with TGF-β1 for 48 hours (32). Co-treatment of PANC1 cells undergoing an EMT with either CTx or Fsk delayed the ability of TGF-β1 to induce an EMT by 48–72 hours, enabling the temporary retention of epithelial properties (Fig S7C, D).

Treatment with CTx or Fsk induced the acquisition of epithelial properties in a range of cell lines that have mesenchymal traits including the Hs578T triple-negative breast cancer cell line (Fig S8A), the SUM149 breast cancer cell line (Fig S8B), the NCI-H596 lung adenosquamous carcinoma cell line (Fig S8C) and the mesenchymal $EpCAM^{lo}$ $CD24^{lo}$ fraction of the EF021 ovarian carcinoma cell line (Fig S8D). Induction of epithelial properties was also observed in PB3 cells (Fig S8E), which constitute an aggressive cell line isolated from mammary tumors of the genetically engineered MMTV-PyMT mouse model of breast cancer, in which the expression of the oncogene is driven by the mouse mammary tumor virus promoter (33). Finally, we note that others have recently reported that forskolin promotes the maintenance of an epithelial morphology in primary human mammary epithelial cells, the absence of which led spontaneously to acquisition of mesenchymal attributes, such as downregulation of E-cadherin expression and upregulation of mesenchymal markers (34).

Taken together, these data signify the importance of PKA signaling in maintaining epithelial characteristics in a variety of normal and neoplastic epithelial cells. These data give an indication that these responses might be a general property of cAMP-induced activation of PKA in the reversal of phenotypes created by activation of an EMT program.

Although CTx was able to induce entrance of the N8 cells and a range of other cell systems into a stably maintained epithelial state, there were a few models in which neither CTx nor Fsk was able to do so, namely the MDA-MB-231 and SUM159 human breast cancer cell lines, amongst others. These cell lines are maintained in the mesenchymal state through the deletion or stable silencing of several key epithelial genomic loci, including the repression of E-cadherin through strong DNA promoter hypermethylation (35). Hence, although the observed effects of PKA activation are applicable to some breast cancer lines and other carcinomas, they are not universal and depend instead on the specific genetic or epigenetic state of the cells.

Essential role of PKA-induced activation of PHF2 in MET

PKA is known to act on many substrates in both the cytoplasm and nucleus (36). Treatment of HMLE and N8 cells with CTx resulted in an immediate increase in the presence of both isoforms of the catalytic subunit in the nucleus (Fig S9A and B), which suggested that PKA might be regulating nuclear substrates following activation by cAMP. The most well-studied substrate of PKA, CREB1, translocates to the nucleus upon phosphorylation by PKA at Ser-133, thereafter altering the transcription of hundreds of target genes (37). In fact, about 300 distinct physiologic stimuli have been described in the literature that can induce CREB Ser-133 phosphorylation (38). It was, therefore, not surprising that CREB was already phosphorylated and present in the nucleus of the N8 cells even prior to their treatment with either CTx or Fsk (Fig 3A). Note that knockdown of CREB1 using at least two shRNAs (Fig S5C) did not affect the ability of CTx to induce an MET in the N8 cells (Fig 3B). Moreover, loss of CREB1 alone induced a partial MET in N8 cells (Fig 3B), consistent with previous reports of its role in the induction of an EMT (39, 40). From these observations, it was obvious that CREB1 did not play an important role in the PKA-induced MET. We then assessed the localization of Gli1, Gli2 and Gli3, which have been previously reported to be PKA substrates that are retained in the cytoplasm following phosphorylation (41), and found no retention of any of the Gli proteins in the cytoplasm following treatment with CTx or Fsk (Fig S9C). These observations indicate that the Gli proteins may not play a role in the observed PKA-induced MET.

Having explored the two most commonly reported nuclear substrates of PKA, we then chose to focus on PHF2, an H3K9 histone demethylase, which is known to become activated upon phosphorylation by PKA (42). We found that knockdown of PHF2 expression in N8 cells using either of two shRNAs (Fig S5B) phenocopied the effects of PKA knockdown in that it prevented CTx-induced mesenchymal-epithelial transition (Fig 3C and D). In contrast, knockdown of PHF2 did not alter the ability of HMLE cells to undergo an EMT (Fig 3F and G), indicating that this enzyme, while necessary for induction of an MET, apparently plays no role in the reverse process -- the EMT, suggesting that it is specifically important for the derepression of silenced epithelial genes through its function as a H3K9 histone demethylase.

PHF2 can be phosphorylated by PKA at four serine residues in its C-terminus (42) (Fig 3E). Accordingly, we engineered a phospho-mimetic form of PHF2 in which all four of these serines were replaced by aspartate residues. While expression of this mutant in N8 cells was not sufficient on its own to induce an MET, the phospho-mimetic PHF2 was able to accelerate the rate of CTx-induced transition from the mesenchymal to the epithelial state from 14 days to 6–7 days (Fig 3H, I). Hence, while PHF2 is essential for MET, it appears to be only one of the effectors of PKA operating during induction of epithelial transition.

To test whether PHF2 can be directly phosphorylated by PKA in our system, we performed an immunoprecipitation of PHF2 followed by immunoblotting using an antibody that recognizes phospho-PKA substrate motif. As shown in Fig 3J, 24 hours after treatment of N8 cells with CTx, phosphorylation of PHF2 by PKA can be observed, providing evidence that PKA phosphorylates PHF2 in the N8 cells. Together these results suggest an important role for PHF2 as a PKA substrate in the induction of an MET.

PKA-induced activation of PHF2 and the epigenetic reprogramming of mesenchymal cells

The H3K9me2 and H3K9me3 marks have been associated with repression of gene transcription (43). Given the previously reported role of PHF2 as an H3K9me2/3 demethylase, we performed chromatin immunoprecipitation followed by deep sequencing (ChIP-Seq) using antibodies against the H3K9me3 and H3K9me2 marks to observe the presence of these marks in untreated N8 cells as well as CTx-treated counterparts in which PHF2 is active. In addition we also performed ChIP-Seq for PHF2, comparing genome-wide occupancy in N8 cells to the N8-CTx cells. We did so in order to monitor PHF2-associated alterations that might enable phenotypic shifts from the mesenchymal to epithelial states, including shifts that might relieve the H3K9-mediated silencing of epithelial genes.

As seen in Fig 4A, there was a striking inverse correlation at specific loci of the presence of PHF2 with the repressive H3K9me2 or H3K9me3 marks. This suggests that presence of this demethylase may, on it own, suffice to relieve histone-mediated transcriptional silencing. As previously reported, PHF2 appears to occupy the promoter region of genes where it recognizes the H3K4me3 histone mark (Fig 4B) (9). Interestingly, the total H3K9me3 counts (greater than 4-fold enrichment above control) in N8-CTx cells was almost half of the total counts of the same mark in N8 cells (35,455 vs 18,675). Similarly, the total H3K9me2 counts in N8-CTx cells were also less than a half of that in the N8 cells (1295 vs 473). As shown in the representative circos plots, these data indicate a widespread loss of H3K9-mediated repression of genomic regions upon treatment of N8 cells with CTx and subsequent activation of PHF2 (Fig 4C).

We then sorted for genomic regions present in the N8-CTx but not N8 cells that contained PHF2 binding and lacked repressive H3K9me2/3 marks (Table S3). This provided us with a list of genomic regions that were relieved of H3K9me2/3-mediated silencing in the N8-CTx cells, as compared to the N8 cells, owing to PHF2 occupancy. To ensure that these changes were specific for the loss of PHF2, we performed ChIP-Seq for H3K9me2/3 and PHF2 in CTx-treated N8 cells that had an shRNA against PHF2 preventing the MET (Table S4). These cells that remained morphologically mesenchymal also demonstrated a similar epigenetic profile to N8 cells with an overlap of 11,807 peaks than the reverted N8-CTx cells, which had an overlap of 6864 peaks. Hence the list of altered genomic regions outlined in Table S3 represents genes that were relieved of H3K9-mediated repression upon CTx-induced activation of PHF2. This suggests that PHF2 activity could be directly responsible for the derepression of these genes that are characteristic of the epithelial cell state. In addition, the expression values of genes that correspond to these genomic loci were also measured in reverted N8-CTx (epithelial) and parental N8 (mesenchymal) cells by RNA-seq which verified that gain of PHF2 occupancy and loss of H3K9 marks did indeed lead to increased expression (Table S3).

Several genes that play a major role in the phenotype and profile of cells in the epithelial state were activated by CTx treatment. Amongst the list of genes that were relieved of silencing upon treatment with CTx include *CDH1* and *CDH3* (among other cadherin genes) that code for E-cadherin and P-cadherin (Fig S10A), respectively, which are essential components of adherens junctions and hallmark proteins of basal epithelial cells; *KRT8* and *KRT18* (Fig S10B), whose gene products are characteristic components of the cytoskeleton

of epithelial cells; and *AJAP1* and *CLDN4* (Fig S10C, D), which specify genes coding for constituents of adherens and tight junctions that are formed by epithelial but not mesenchymal cells. Other regions include the *TP63* gene (Fig S10E) whose product is a hallmark transcription factor of basal mammary epithelial cells and *ITGB2*, *ITGB6* (Fig S10F) and *ITGB8*, which code for integrins that are typically expressed on epithelial cells.

These observations reveal a mechanism by which activation of this demethylase enables the transcription of genes that induce an MET and ultimately define the state of the cells.

Activation of PKA and the differentiation of TICs in vivo

We tested the tumor-initiating ability of cells that have been induced to undergo an MET by activation of PKA in vitro. We transplanted at limiting dilutions the neoplastic, *RAS*-transformed derivatives of HMLE, N8 and the reverted N8-CTx cells, termed HMLE-Ras, N8-Ras, and N8-CTx-Ras, into the mammary fat pads of NOD/SCID mice. As anticipated, the frequency of tumor-initiating cells in the N8-Ras cells was far greater than in the HMLE-Ras cell population, in this case 100-fold higher. Significantly, the N8-CTx-Ras cells were as inefficient at tumor-initiation as the HMLE-Ras cells (Fig 5A). The primary tumors that arose upon orthotopic mammary stromal fat pad implantation of N8-Ras tumors spawned 20 to 30 micrometastases in the lungs by 12 weeks following implantation. This property was completely lost upon induction of an MET by CTx treatment prior to transplantation (Fig 5C and Fig S11A), which nevertheless formed primary tumors of comparable size (Fig 5B). Moreover, this confirmed previous observations that the phenotypic state of these cells prior to neoplastic transformation strongly influenced their behavior following transformation.

To better mimic a clinical scenario, we next asked how the induction of an MET would impact pre-established tumors derived from mesenchymal N8 cells. While we wished to pharmacologically treat mice that already had established N8-Ras tumors, CTx is too toxic to be administered systemically, and the rapid clearance and poor pharmacodynamics of Fsk made it difficult to study its effects upon systemic administration. Such difficulties in treating mice with PKA agonists have also been reported previously (44, 45). For this reason, we focused our efforts on studying the proof-of-principle effects of PKA activation *in vivo* using the doxycycline-inducible version of constitutively active PKA (caPKA). Thus, we induced expression of the caPKA in already-formed N8-Ras tumors of 5mm diameter (Fig 5D). Upon visual inspection, the tumors that had been exposed for 14 days to doxycycline contained pasty, fluid-filled necrotic cores when compared to the tumors that had never been exposed to doxycycline, the latter being solid with a hard center of viable cells. Tumors from mice that received doxycycline weighed less than those that did not receive any (Fig 5F). Moreover, those tumors in which expression of caPKA had been induced developed a more differentiated histomorphology as revealed by H&E staining of tumor sections (Fig S11B, C). Importantly, when tumors were harvested and subjected to FACS analysis, the doxycycline-treated tumors showed a decrease in expression of the CD44 cell-surface marker associated with the stem-like population (20) in contrast to the untreated tumors (Fig S11D).

Strikingly, secondary transplantation of cells isolated from the doxycycline-exposed tumors at limiting dilutions revealed a ~20-fold loss of tumor-initiating ability (Fig 5E), showing

that activation of PKA induces differentiation of TICs, diminishing their ability to subsequently seed new tumors. This result demonstrates that constitutive expression of PKA for a 14-day period in a growing tumor suffices on its own to induce the differentiation of TICs in the tumor, reducing the tumor-initiating properties of its associated cells as indicated by their subsequent inability to propagate tumors upon secondary transplantation.

Discussion

Cyclic AMP and its main effector, PKA, have been studied for four decades in a variety of cell-biological and physiologic settings, where its effects in activating a number of distinct, tissue-specific traits have been repeatedly documented (11). A role that it might play in governing the epithelial cell state and thus suppressing entrance into the alternative mesenchymal state in breast cancers has not been described. The present work makes its clear that this second messenger and its main effector, PKA, play a key role in determining this epithelial versus mesenchymal balance of mammary epithelial cells, as well as epithelial cells of other tissues. Indeed, in light of these results, it becomes plausible that maintenance of the residence of cells in an epithelial state depends on tonic elevated levels of intracellular cAMP. In retrospect, it now seems likely that the use of cholera toxin as an ingredient in the tissue culture medium of various epithelial cell types (including cells of the epidermis, mammary gland and bronchus (46, 47)) was motivated by the observation that loss of such cells in culture was accompanied by an overgrowth of fibroblast-like cells (46).

These results collectively indicate a role for PKA in the differentiation of TICs by enforcing residence in the epithelial state and preventing or reversing the EMT program. Although PKA can act via a large number of substrates, we identified PHF2 as an important downstream effector of PKA that mediates the induction of epithelial characteristics through epigenetic reprogramming to a chromatin state that is more favorable for residence in the epithelial state. We find that activating this histone demethylase enables PKA to induce the transcription of genes that play a role in the entrance into and maintenance of residence in the epithelial state.

The EMT program is known to represent one defined route for the generation of both normal and neoplastic epithelial stem cells (6, 7, 48). The observations that PKA-induced activation of PHF2 can either reverse or curtail this program present an opportunity to exploit such a mechanism for therapeutic gain. Indeed the differentiation of TICs through the induction of an MET is an attractive proposition - one that could be pursued through the induced increase of intracellular cAMP levels, activation of PKA, or activation of PHF2. Nonetheless, it is likely that many such approaches will result in widespread side-effect toxicities owing to the multitude of signaling pathways that are activated downstream of cAMP increase (11). Specific activation of the PHF2 histone-modifier enzyme may serve as a means of derepressing genes that are essential for the differentiated epithelial state without eliciting many of the toxicities of induced cAMP increases. Along the same lines, identification of a histone methyltransferase that counteracts PHF2 function may also provide an attractive target for therapeutic inhibition, a strategy that has proven successful in the case of DOT1L inhibition against MLL-driven leukemias (49). The role of the G9a histone

methyltransferase in establishing the H3K9me2 mark for repression of the *CDH1* promoter in breast cancer cells has been reported previously (50).

This study provides mechanistic insight into the benefits of targeting such an enzyme in epithelial tumors, preventing the constituent cells from undergoing an EMT and thereby acquiring aggressive characteristics, including increases in the numbers of TICs. The pathways explored in this study provide novel insight into the functions of PKA in the induction of an MET and the differentiation of the more aggressive TICs within a tumor. This study reveals a new direction for targeting the TIC population through epigenetic rewiring that ultimately results in their differentiation and increased susceptibility to conventional chemotherapeutic drugs.

Materials and Methods

Cell Culture and treatments

HMLE, NAMEC8 and all derived cell lines were grown in MEGM medium (Lonza, USA), MCF10A cells were grown in DMEM/F12 containing 5% horse serum (Sigma USA; H0146), EGF 20ng/mL, Hydrocortisone 0.5mg/mL, Cholera Toxin 100ng/mL and insulin 10μg/mL. EF021 and H596 cells were grown in RPMI containing 10% fetal bovine serum. MCF7Ras cells were grown in DME containing 10% fetal bovine serum. Hs578T were grown in DME containing 10% fetal bovine serum and 10μg/mL insulin. Cells were treated with either 100ng/mL of Cholera Toxin (Calbiochem USA; 227036), which was replenished every two days, or 1uM Forskolin (Tocris Biosciences USA; 1099), which was replenished daily over a period of 14 days. Cells were split to a ratio of 1:6 every 3 days during the treatments.

Screening

For the *CDH1* reporter screen 500 N8 cells bearing *wtCDH1* promoter luciferase were seeded into 384-well plates in a volume of 40ul. 24h later, 100nl of each compound (200uM stock) were added using a CyBio liquid handler, resulting in a final screen concentration of 0.5uM. Four days later, the plates were read for either firefly luciferase activity (Pierce, Cat# 16177) or CellTiter Glo (Promega USA, Cat# G7572). The Enzo compound library (Plate A and Plate B; 451 compounds, including repeats) was obtained from the Koch Institute Screening Facility at MIT. Firefly luciferase and CellTiter Glo assays were performed in triplicates.

The vulnerabilities of the reverted cells were assessed by screening against the Selleck anti-cancer compound library (400 compounds) and the Enzo kinase library (80 compounds) at the Koch Institute Screening Facility at MIT. 1000 N8 or N8-CTx cells were seeded in 384-well plates in a volume of 50ul. 24h later, 50nl of each compound was added to assay a 5-point dose response. Three days later, the plates were read for CellTiter Glo, assays were performed in duplicate.

Flow Cytometry

Cells were prepared according to standard protocols and suspended in 2% IFS/PBS. DAPI (Life Technologies USA; D1306) was used to exclude dead cells. Cells were sorted on BD FACSAria SORP and analysed on BD LSRII, using BD FACSDiva Software (BD Biosciences, USA). Antibodies used were anti- CD44-PE-Cy7 (Biolegend USA #103029), anti- CD24-PE (BD Biosciences USA #555428), anti-CD45-Pacific Blue (Biolegend USA #103125), anti-CD31-Pacific Blue (Biolegend USA #102421).

Mammosphere/Tumorsphere Culture

Mammosphere/tumorsphere culture was performed as previously described (51). 1000 cells were seeded per well of a 96-well Corning Ultra-Low attachment plate (Corning USA; CLS3474) in replicates of 10, sphere numbers were counted between days 8 to 12.

Migration and Invasion Assays

Twenty-five thousand cells were seeded into 24-well cell culture inserts with 8 μm pores (BD Falcon, USA). After 12 to 24 hours, the cells on the upper surface of the filters were removed with a cotton swab. For visualization, cells on lower filter surfaces were fixed and stained with a Diff-Quick staining kit (Dade Behring/Siemens, Germany). Three to five fields per filter were counted. Data are presented as migrated cells per field.

RNA preparation and qRT-PCR analysis

Total RNA was isolated using the RNeasy Plus Mini kit (Qiagen USA; 74136) and reverse transcription was performed with the High Capacity RNA-to-cDNA Kit (Life Technologies USA; 4387406), both according to the manufacturer's protocols. A cDNA sample prepared from 1 μg total RNA was used for quantitative RT-PCR. The PCR reactions were performed using the Fast SYBR Green Master Mix (Life Technologies; 4385612), data collection and data analysis were performed on the ABI7900 machine (Applied Biosystems, USA) using the SDS2.0 and RQ manager software. The thermal cycling parameters for the PCR were as follows: 95 °C for 5 min, followed by 45 cycles of 95 °C for 10 sec, 49 °C for 7 sec, and 72 °C for 25 sec. The relative mRNA quantity was normalized against the relative quantity of HPRT1 mRNA in the same sample.

Name	Primer sequence in 5'-3' orientation
E-CADHERIN	F – TTGCACCGGTCGACAAAGGAC R - TGGATTCCAGAAACGGAGGCC
FIBRONECTIN	F - GAGAATGGACCTGCAAGCCCA R - AGTGCAAGTGATGCGTCCGC
VIMENTIN	F – ACCCGCACCAACGAGAAGGT R - ATTCTGCTGCTCCAGGAAGCG
SNAI1	F - CTGGGTGCCCTCAAGATGCA R - CCGGACATGGCCTTGTAGCA
SNAI2	F – TACCGCTGCTCCATTCCACG R - CATGGGGGTCTGAAAGCTTGG
TWIST1	F - TGCGGAAGATCATCCCCACG

Name	Primer sequence in 5’-3’ orientation
	R - GCTGCAGCTTGCCATCTTGGA
ZEB1	F – TGCACTGAGTGTGGAAAAGC R - TGGTGATGCTGAAAGAGACG
HPRTI	F- CTCCGTTATGGCGACCC R- CACCCT TTCCAAATCCTCAG
PHF2	F- CCCATGGGTTTTCTCACAGT R- GGCTCCCCTACGACGTTA
PRKACA	F- GTGTTCTGAGCGGGACTTTC R- GCCCTGAGAACAGGACTGAG
PRKACB	F- AAAGTCTTCTTTGGCTTTGGC R- CCTTCCCTGACCCCTTCTT

Immunofluorescence (cultured cells)

Cells were cultured on dishes containing coverslips for 2–3 days following which coverslips were washed in cold PBS, fixed in 4% paraformaldehyde for 10 minutes at 4°C and permeabilized in 0.2% tritonX in PBS for 2 minutes. Cells were then washed in PBS, blocked for 1 hour at room temperature in PBS containing 3% normal horse serum (Vector Labs USA; S-2000). Fixed cells were then incubated with the primary antibody in PBS containing 1%BSA solution overnight at 4°C. Cells were washed in PBS three times and secondary antibody was added in PBS containing 1%BSA solution for 1–2 hours at room temperature in the dark. Cells were washed three times in PBS and were incubated for 2 minutes in DAPI solution, following which they were washed in PBS and mounted with a drop of Prolong Gold antifade reagent (Life Technologies USA; P36961) and coverslipped. Slides were imaged on a PerkinElmer Ultraview Spinning Disk Confocal and analyzed using Volocity software.

Immunofluorescence (Tissue microarrays)

Slides were rehydrated by incubating in Histoclear solution twice for 5 minutes each, followed by incubation in 100% ethanol twice for 5 minutes each, in 95% ethanol twice for 5 minutes each, 70% ethanol twice for five minutes each, once in 35% ethanol for five minutes and in water for 5 minutes. Pressure cooker mediated heat induced epitope retrieval was carried out in 250mL of unmasking buffer containing sodium citrate at pH 6. Following retrieval, slides were blocked for 30 minutes in PBS containing 3% normal horse serum following which they were incubated with primary antibody in blocking solution overnight at 4°C. Slides were washed twice with PBS and incubated with secondary antibody at room temperature for 1 hour in the dark. Following two PBS washes, 20ul of mounting medium was added, coverslipped and stored in the dark for 24 hours before imaging.

Target	Company	Catalog #	host	Dilution
E-Cadherin	BD Biosciences	610182	mouse	1:500
E-Cadherin	Cell Signaling Technologies	3195	rabbit	1:200
Fibronectin	BD Biosciences	610078	mouse	1:200

Target	Company	Catalog #	host	Dilution
PKAC-α	Cell Signaling Technologies	4782	rabbit	1:100
PKAC- α	Abcam	ab124390	mouse	10 μg/ml
PKAC-β	Santa Cruz Biotechnology	sc-904	rabbit	1:100
Vimentin	Cell Signaling Technologies	3932	rabbit	1:100
PHF2	Abcam	ab154983	mouse	1:50

Proliferation Assays

To measure rate of proliferation, 1000 cells were seeded onto 96-well plate in quadruplicate. Proliferation was measured using CyQuant (Life Technologies USA, C7026) according to manufacturer's protocols.

Protein Extraction and Western Blotting

To obtain protein extracts, cells were washed with chilled PBS and scraped from culture dishes in aqueous lysis buffer (50mM Tris pH7.5, 150mM NaCl, 10mM EDTA pH8.0, 0.2% Sodium Azide, 50mM NaF, 0.5% NP40) containing cOmplete mini protease inhibitor cocktail (Roche, USA 04693159001) and stored at −80°C. Following thawing, they were centrifuged at top speed on a benchtop centrifuge at 4°C for 20 minutes and the supernatant was assayed for protein concentration with Bradford Reagent (Bio-Rad; 500-0006). 30ug of total protein were separated by SDS-PAGE on NuPage gels (Invitrogen, USA) and transferred to Hybond-P PVDF membrane (GE Healthcare, USA). Membranes were probed with specific primary antibodies and antibody-protein complex detected by HRP-conjugated secondary antibodies and SuperSignal West Dura Extended Duration Substrate (Life Technologies USA; 34075).

Target	Company	Catalog #	host	Dilution
E-Cadherin	Cell Signaling Technology	3195	rabbit	1:1000
Fibronectin	BD Biosciences	610078	mouse	1:1000
PKAC-α	Cell Signaling Technology	4782	rabbit	1:1000
PKAC-β	Santa Cruz Biotechnology	sc-904	rabbit	1:1000
Zeb1	Cell Signaling Technology	3396	rabbit	1:1000
Snail1	Cell Signaling Technology	3879	rabbit	1:1000
Vimentin	Cell Signaling Technology	3932	rabbit	1:1000
PHF2	Abcam	ab154983	mouse	1:500
P-CREB1	Cell Signaling Technology	9198	rabbit	1:1000
CREB1	Cell Signaling Technology	9197	rabbit	1:1000
Gli1	Santa Cruz Biotechnology	sc-20687	rabbit	1:1000
Gli2	Santa Cruz Biotechnology	sc-271786	mouse	1:1000
Gli3	Santa Cruz Biotechnology	sc-6154	goat	1:1000
p-PKA substrate	Cell Signaling Technology	9621	rabbit	1:1000

Target	Company	Catalog #	host	Dilution
PHF2	Cell Signaling Technology	3497	rabbit	1:1000
Cox IV	Cell Signaling Technology	4850	rabbit	1:1000

Immunoprecipitation

N8 cells in 15cm dishes were scraped and harvested in 0.5mL ice-cold IP buffer (Cell Signaling Technology, USA) containing protease and phosphatase inhibitors (Roche, Germany) following which they were sonicated with three pulses on ice. Lysates were spun down at 14,000g for 10 minutes and supernatants collected for IP. Anti-PHF2 antibody (Catalog# 3497; Cell Signaling Technology, USA) was added at 1:25 and incubated overnight at 4°C rotating. The following morning, 40ul of magnetic protein A/G beads (Catalog #26162; Thermo Scientific, USA) were added, incubated for 30 minutes on a rotator following which beads were washed 5 times using a magnetic separator with cold IP buffer. Beads were then boiled in LDS buffer and run on an SDS-PAGE gel followed by immunoblotting.

RNAi-mediated knockdown

To generate shRNA expressing plasmids, double-stranded oligonucleotides (oligos) encoding the desired shRNA were cloned into a Tet-pLKO-puro lentiviral vector (Addgene, plasmid 21915). In the absence of doxycycline, shRNA expression is repressed by constitutively expressed TetR protein. Upon the addition of doxycycline to the growth media, shRNA expression is triggered resulting in target gene knock-down. The cloning vector has a 1.9 kb stuffer that is released by digestion with AgeI and EcoRI. shRNA oligos are cloned into the AgeI and EcoRI sites in place of the stuffer.

PKA hairpins

Name	Target Sequence	**Forward Oligo - full sequence 5’ flank sequence: CCGG Loop sequence: CTCGAG 3’ flank sequence: TTTTTG**	**Reverse Oligo - full sequence 5’ flank sequence: AATTCAAAAA Loop sequence: CTCGAG 3’ flank sequence: (none)**
A1	CCCTTCATACCAAAGTTTAAA	5’-CCGGCCCTTCATACCAAAGTTTAAACTCGAGTTTAAACTTTGGTATGAAGGGTTTTTG-3’	5’-AATTCAAAAACCCTTCATACCAAAGTTTAAACTCGAGTTTAAACTTTGGTATGAAGGG-3’
B1	GACCAACCAATTCAGATTTAT	5’-CCGGGACCAACCAATTCAGATTTATCTCGAGATAAATCTGAATTGGTTGGTCTTTTTG-3’	5’-AATTCAAAAAGACCAACCAATTCAGATTTATCTCGAGATAAATCTGAATTGGTTGGTC-3’
B3	GTCTCAATAAGGCAATATATT	5’-CCGGGTCTCAATAAGGCAATATATTCTCGAGAATATATTGCCTTATTGAGACTTTTTG-3’	5’-AATTCAAAAAGTCTCAATAAGGCAATATATTCTCGAGAATATATTGCCTTATTGAGAC-3’
B4	AGACCAACCAATTCAGATTTA	5’-CCGGAGACCAACCAATTCAGATTTACTCGAGTAAATCTGAATTGGTTGGTCTTTTTTG-3’	5’-AATTCAAAAAAGACCAACCAATTCAGATTTACTCGAGTAAATCTGAATTGGTTGGTCT-3’
B10	GTCATGTAAATGCTGATATTG	5’-CCGGGTCATGTAAATGCTGATAT	5’-AATTCAAAAAGTCATGTAAATGC

Name	Target Sequence	Forward Oligo - full sequence 5’ flank sequence: CCGG Loop sequence: CTCGAG 3’ flank sequence: TTTTTG	Reverse Oligo - full sequence 5’ flank sequence: AATTCAAAAA Loop sequence: CTCGAG 3’ flank sequence: (none)
		TGCTCGAGCAATATCAGCATTTACATGACTTTTTG-3’	TGATATTGCTCGAGCAATATCAGCATTTACATGAC-3’
B12	GTTTAGAGGCTCTGGAGATAC	5’-CCGGGTTTAGAGGCTCTGGAGATACCTCGAGGTATCTCCAGAGCCTCTAAACTTTTTG-3’	5’-AATTCAAAAAGTTTAGAGGCTCTGGAGATACCTCGAGGTATCTCCAGAGCCTCTAAAC-3’

PHF2 hairpins

Name	Target Sequence	Forward Oligo	Reverse Oligo
P1	GGAGCCACCTGACATTGTAAA	5’-CCGGGGAGCCACCTGACATTGTAAACTCGAGTTTACAATGTCAGGTGGCTCCTTTTTG-3’	5’-AATTCAAAAAGGAGCCACCTGACATTGTAAACTCGAGTTTACAATGTCAGGTGGCTCC-3’
P3	TTGCTGACCAGGTCGACAAAT	5’-CCGGTTGCTGACCAGGTCGACAAATCTCGAGATTTGTCGACCTGGTCAGCAATTTTTG-3’	5’-AATTCAAAAATTGCTGACCAGGTCGACAAATCTCGAGATTTGTCGACCTGGTCAGCAA-3’

CREB1 hairpins

Name	Target Sequence
CREB1	ACGGTGCCAACTCCAATTTAC
CREB3	ACAGCACCCACTAGCACTATT

Animal Studies

Research involving animals complied with protocols approved by the MIT Committee on Animal Care. For tumor studies, cells suspended in 15μl 30% Matrigel(GFR)/PBS mix (BD Biosciences; 356230) were injected into the inguinal mammary gland fat pads of age-matched female NOD/SCID mice (Jackson Laboratory). Mice were sacrificed after 10 weeks or when tumors reached a diameter >1 cm. Lung surface metastases were counted with a fluorescent microscope.

Chromatin Immunoprecipitation followed by Sequencing

ChIP for PHF2, H3K9me2 and H3K9me3 was carried out using the SimpleChIP® Plus Enzymatic Chromatin IP Kit (Catalog# 9005; Cell Signaling Technology, USA) and the protocols within. The PHF2 rabbit monoclonal antibody (Catalog#3497; Cell Signaling Technology, USA) was used at 1:25 per IP, the H3K9me2 mouse monoclonal (Catalog# ab1220; Abcam, USA) and the H3K9me3 rabbit polyclonal antibodies (Catalog#ab8898) were used at 1:50 (10ug) per IP. The ChIP DNA was used to prepare libraries for sequencing, which was carried out in the Genome Technology Core at the Whitehead Institute.

Library Preparation for Sequencing

To prepare libraries for RNA-Seq, the TruSeq stranded mRNA protocol was followed to prep the libraries as described in the kit (Catalog # RS-122–2101, Illumina, USA) manual. To prepare libraries for the ChIP-Seq, the TruSeq ChIP protocol was followed as described in the kit (Catalog # IP-202–1012, Illumina, USA) manual.

Deep Sequencing and data analysis

Sequencing: Libraries were pooled together and sequenced on the HiSeq 2500 sequencer using the Standard sequencing protocols. Images analysis and base calling was done using the Standard Illumina pipeline, and then demultiplexed into fastq files. RNASeq paired-end reads from Illumina 1.5 encoding were aligned using TopHat (v 2.0.13) (52) to the human genome (GRCh37) with Ensembl annotation (GRCh37.75) in gtf format. Differential expression was assayed using HTSeq count (53) and DESeq (54). ChIPSeq data were aligned to the human genome (GRCh37) using Bowtie2 (v 2.2.5) (55), base encoding as above, and peaks were called using MACS2 (v 2.1.0.20150420) (56) with *--nomodel* option and fragment length was determined by strand cross-correlation (using phantompeakqualtools https://code.google.com/p/phantompeakqualtools/). Differential binding was determined using MACS' bdgdiff tool. Peaks were annotated using Cis-regulatory Element Annotation System (CEAS) (57), and ChIPSeq data profiles were viewed in ngsplot (58). Overlap between peaks, and with expression data, were determined using bedtools (59). ChIPSeq data profiles were viewed in ngsplot (58) and IGV (60).

RNA-seq and ChIP-seq data have been submitted to GEO and are awaiting a GSE ID.

LC/MS-based metabolite profiling

LC/MS analyses were conducted on a QExactive benchtop orbitrap mass spectrometer equipped with an Ion Max source and a HESI II probe, which was coupled to a Dionex UltiMate 3000 UPLC system (Thermo Fisher Scientific, San Jose, CA). External mass calibration was performed using the standard calibration mixture every 7 days. Polar metabolites were extracted using 1 ml of ice cold 80% methanol with 10 ng/ml phenylalanine-d_8 or phenylalanine-$^{13}C_9$-^{15}N as an internal standard. After 10 min vortex and centrifugation for 10 min at 10,000g, both at 4°C, samples were dried in a centrifugal evaporator. Dried samples were stored at −80°C and then resuspended in 100 µL water; 2.5 µl of each sample was injected onto a ZIC-pHILIC 2.1 × 150 mm (5 µm particle size) column (EMD Millipore). Buffer A was 20 mM ammonium carbonate, 0.1% ammonium hydroxide; buffer B was acetonitrile. The chromatographic gradient was run at a flow rate of 0.150 ml/min as follows: 0–20 min.: linear gradient from 80% to 20% B; 20–20.5 min.: linear gradient from 20% to 80% B; 20.5–28 min.: hold at 80% B. The column oven was held at 25°C. The mass spectrometer was operated with the spray voltage set to 3.0 kV, the heated capillary held at 275°C, and the HESI probe held at 350°C; the sheath gas flow was set to 40 units, the auxiliary gas flow was set to 15 units, and the sweep gas flow was set to 1 unit. To measure cAMP, a positive targeted SIM (tSIM) scan was performed at a resolution of 70,000, an AGC target of 1e5, and the maximum injection time at 250 msec. The tSIM window was set to a width of 1.0 m/z and centered at 330.05980 m/z, corresponding to the [M+H] ion of cAMP. To monitor other endogenous polar metabolites and the internal

standard, the tSIM scans were interspersed with positive and negative mode scans in the range of 70–1000 m/z, with the resolution set to 70,000, the AGC target at 10 , and the maximum injection time at 80 msec. Relative quantitation of polar metabolites was performed with XCalibur QuanBrowser 2.2 (Thermo Fisher Scientific) using a 5 ppm mass tolerance and referencing an in-house library of chemical standards.

Statistical Analysis

Data are presented as mean ± SD. A Student's t test (two-tailed) was used to compare two groups ($p < 0.05$ was considered significant) unless otherwise indicated.

Supplementary Material

Refer to Web version on PubMed Central for supplementary material.

Acknowledgments

We thank the Keck Microscopy Facility, Metabolite Profiling Core Facility, Genome Technology Core, Bioinformatics and Research Computing Core and the Proteomics Core Facility at the Whitehead Institute and the Koch Institute Swanson Biotechnology Center (SBC), specifically the Histology Facility and the High Throughput Screening Facility. We are grateful for John Benson (SBC) for providing the compound library, Dr. Daniel Bachovchin (Broad Institute) for assistance with automation and Mr. Tom DiCesare for assistance with scientific illustration. We would like to thank Dr. Anushka Dongre, Dr. Sonia Iyer, and Ms. Julia Fröse for technical assistance, all members of the Weinberg Lab for helpful discussions and Dr. Arthur Lambert, Dr. Keerthana Krishnan and Dr. Satyaki Rajavasireddy for critical reading of the manuscript. D.R.P is supported by a C. J. Martin Overseas Biomedical Fellowship from the National Health and Medical Research Council of Australia (NHMRC APP1071853). W.L.T is supported by the National Research Foundation, Singapore (NRF-NRFF2015-04) and National Medical Research Council, Singapore (NMRC/TCR/007-NCC/2013). This research was supported by the Ludwig Center for Molecular Oncology at MIT (R.A.W), Breast Cancer Research Foundation (R.A.W), Samuel Waxman Cancer Research Foundation (R.A.W) and the National Institutes of Health R01-CA078461 (R.A.W). R.A.W. is an American Cancer Society and D. K. Ludwig Foundation Cancer Research Professor. R.A.W is a shareholder in and advisor to Verastem Inc. Whitehead Institute has filed a patent application on the subject matter of this manuscript. RNA-Seq and ChIP-Seq data from this study have been deposited at GEO under accession number GSE74883.

REFERENCES AND NOTES

1. Gupta PB, et al. Identification of selective inhibitors of cancer stem cells by high-throughput screening. Cell. 2009 Aug 21.138:645. [PubMed: 19682730]
2. Chen J, et al. A restricted cell population propagates glioblastoma growth after chemotherapy. Nature. 2012 Aug 23.488:522. [PubMed: 22854781]
3. Kreso A, Dick JE. Evolution of the cancer stem cell model. Cell stem cell. 2014 Mar 6.14275
4. Pattabiraman DR, Weinberg RA. Tackling the cancer stem cells - what challenges do they pose? Nature reviews. Drug discovery. 2014 Jul 1.13:497.
5. De Craene B, Berx G. Regulatory networks defining EMT during cancer initiation and progression. Nature reviews. Cancer. 2013 Feb.13:97. [PubMed: 23344542]
6. Mani SA, et al. The epithelial-mesenchymal transition generates cells with properties of stem cells. Cell. 2008 May 16.133:704. [PubMed: 18485877]
7. Morel AP, et al. Generation of breast cancer stem cells through epithelial-mesenchymal transition. PloS one. 2008; 3:e2888. [PubMed: 18682804]
8. Chen C, et al. Evidence for epithelial-mesenchymal transition in cancer stem cells of head and neck squamous cell carcinoma. PloS one. 2011; 6:e16466. [PubMed: 21304586]
9. Ahmed N, Abubaker K, Findlay J, Quinn M. Epithelial mesenchymal transition and cancer stem cell-like phenotypes facilitate chemoresistance in recurrent ovarian cancer. Current cancer drug targets. 2010 May.10:268. [PubMed: 20370691]

10. Beavo JA, Brunton LL. Cyclic nucleotide research -- still expanding after half a century. Nat Rev Mol Cell Biol. 2002 Sep.3:710. [PubMed: 12209131]
11. Tasken K, Aandahl EM. Localized effects of cAMP mediated by distinct routes of protein kinase A. Physiological reviews. 2004 Jan.84:137. [PubMed: 14715913]
12. Taylor SS, Ilouz R, Zhang P, Kornev AP. Assembly of allosteric macromolecular switches: lessons from PKA. Nature reviews. Molecular cell biology. 2012 Oct.13:646. [PubMed: 22992589]
13. MacPherson MR, et al. Phosphorylation of serine 11 and serine 92 as new positive regulators of human Snail1 function: potential involvement of casein kinase-2 and the cAMP-activated kinase protein kinase A. Molecular biology of the cell. 2010 Jan 15.21:244. [PubMed: 19923321]
14. Shaikh D, et al. cAMP-dependent protein kinase is essential for hypoxia-mediated epithelial-mesenchymal transition, migration, and invasion in lung cancer cells. Cellular signalling. 2012 Dec.24:2396. [PubMed: 22954688]
15. Nadella KS, et al. Targeted deletion of Prkar1a reveals a role for protein kinase A in mesenchymal-to-epithelial transition. Cancer research. 2008 Apr 15.68:2671. [PubMed: 18413734]
16. Amieux PS, et al. Increased basal cAMP-dependent protein kinase activity inhibits the formation of mesoderm-derived structures in the developing mouse embryo. The Journal of biological chemistry. 2002 Jul 26.277:27294. [PubMed: 12004056]
17. Iglesias-Bartolome R, et al. Inactivation of a Galpha(s)-PKA tumour suppressor pathway in skin stem cells initiates basal-cell carcinogenesis. Nature cell biology. 2015 Jun.17:793. [PubMed: 25961504]
18. Li X, et al. Intrinsic resistance of tumorigenic breast cancer cells to chemotherapy. Journal of the National Cancer Institute. 2008 May 7.100:672. [PubMed: 18445819]
19. Elenbaas B, et al. Human breast cancer cells generated by oncogenic transformation of primary mammary epithelial cells. Genes & development. 2001 Jan 1.15:50. [PubMed: 11156605]
20. Al-Hajj M, Wicha MS, Benito-Hernandez A, Morrison SJ, Clarke MF. Prospective identification of tumorigenic breast cancer cells. Proceedings of the National Academy of Sciences of the United States of America. 2003 Apr 1.100:3983. [PubMed: 12629218]
21. Tam WL, et al. Protein kinase C alpha is a central signaling node and therapeutic target for breast cancer stem cells. Cancer cell. 2013 Sep 9.24:347. [PubMed: 24029232]
22. Onder TT, et al. Loss of E-cadherin promotes metastasis via multiple downstream transcriptional pathways. Cancer research. 2008 May 15.68:3645. [PubMed: 18483246]
23. Anastassiou D, et al. Human cancer cells express Slug-based epithelial-mesenchymal transition gene expression signature obtained in vivo. BMC cancer. 2011; 11:529. [PubMed: 22208948]
24. Charafe-Jauffret E, et al. Gene expression profiling of breast cell lines identifies potential new basal markers. Oncogene. 2006 Apr 6.25:2273. [PubMed: 16288205]
25. de Rooij J, et al. Epac is a Rap1 guanine-nucleotide-exchange factor directly activated by cyclic AMP. Nature. 1998 Dec 3.396:474. [PubMed: 9853756]
26. Broillet MC, Firestein S. Cyclic nucleotide-gated channels. Molecular mechanisms of activation. Annals of the New York Academy of Sciences. 1999 Apr 30.868:730. [PubMed: 10414360]
27. Meyer RB Jr, Miller JP. Analogs of cyclic AMP and cyclic GMP: general methods of synthesis and the relationship of structure to enzymic activity. Life sciences. 1974 Mar 16.14:1019. [PubMed: 4362776]
28. Enserink JM, et al. A novel Epac-specific cAMP analogue demonstrates independent regulation of Rap1 and ERK. Nature cell biology. 2002 Nov.4:901. [PubMed: 12402047]
29. Orellana SA, McKnight GS. Mutations in the catalytic subunit of cAMP-dependent protein kinase result in unregulated biological activity. Proc Natl Acad Sci U S A. 1992 May 15.89:4726. [PubMed: 1584809]
30. Soule HD, et al. Isolation and characterization of a spontaneously immortalized human breast epithelial cell line, MCF-10. Cancer research. 1990 Sep 15.50:6075. [PubMed: 1975513]
31. Sommers CL, Papageorge A, Wilding G, Gelmann EP. Growth properties and tumorigenesis of MCF-7 cells transfected with isogenic mutants of rasH. Cancer research. 1990 Jan 1.50:67. [PubMed: 2403419]

32. Ellenrieder V, et al. Transforming growth factor beta1 treatment leads to an epithelial-mesenchymal transdifferentiation of pancreatic cancer cells requiring extracellular signal-regulated kinase 2 activation. Cancer research. 2001 May 15.61:4222. [PubMed: 11358848]
33. Guy CT, Cardiff RD, Muller WJ. Induction of mammary tumors by expression of polyomavirus middle T oncogene: a transgenic mouse model for metastatic disease. Molecular and cellular biology. 1992 Mar.12:954. [PubMed: 1312220]
34. Linnemann JR, et al. Quantification of regenerative potential in primary human mammary epithelial cells. Development. 2015 Jun 12.
35. Hollestelle A, et al. Distinct gene mutation profiles among luminal-type and basal-type breast cancer cell lines. Breast cancer research and treatment. 2010 May.121:53. [PubMed: 19593635]
36. Shabb JB. Physiological substrates of cAMP-dependent protein kinase. Chemical reviews. 2001 Aug.101:2381. [PubMed: 11749379]
37. Gonzalez GA, Montminy MR. Cyclic AMP stimulates somatostatin gene transcription by phosphorylation of CREB at serine 133. Cell. 1989 Nov 17.59:675. [PubMed: 2573431]
38. Johannessen M, Delghandi MP, Moens U. What turns CREB on? Cellular signalling. 2004 Nov. 16:1211. [PubMed: 15337521]
39. Wu D, et al. cAMP-responsive element-binding protein regulates vascular endothelial growth factor expression: implication in human prostate cancer bone metastasis. Oncogene. 2007 Aug 2.26:5070. [PubMed: 17310988]
40. Singh R, Shankar BS, Sainis KB. TGF-beta1-ROS-ATM-CREB signaling axis in macrophage mediated migration of human breast cancer MCF7 cells. Cellular signalling. 2014 Jul.26:1604. [PubMed: 24705025]
41. Sheng T, Chi S, Zhang X, Xie J. Regulation of Gli1 localization by the cAMP/protein kinase A signaling axis through a site near the nuclear localization signal. The Journal of biological chemistry. 2006 Jan 6.281:9. [PubMed: 16293631]
42. Baba A, et al. PKA-dependent regulation of the histone lysine demethylase complex PHF2-ARID5B. Nature cell biology. 2011 Jun.13:668. [PubMed: 21532585]
43. Hublitz P, Albert M, Peters AH. Mechanisms of transcriptional repression by histone lysine methylation. The International journal of developmental biology. 2009; 53:335. [PubMed: 19412890]
44. Saunders MP, et al. A novel cyclic adenosine monophosphate analog induces hypercalcemia via production of 1,25-dihydroxyvitamin D in patients with solid tumors. The Journal of clinical endocrinology and metabolism. 1997 Dec.82:4044. [PubMed: 9398710]
45. Propper DJ, et al. Phase I study of the novel cyclic AMP (cAMP) analogue 8-chloro-cAMP in patients with cancer: toxicity, hormonal, and immunological effects. Clinical cancer research : an official journal of the American Association for Cancer Research. 1999 Jul.5:1682. [PubMed: 10430069]
46. Taylor-Papadimitriou J, Purkis P, Fentiman IS. Cholera toxin and analogues of cyclic AMP stimulate the growth of cultured human mammary epithelial cells. Journal of cellular physiology. 1980 Mar.102:317. [PubMed: 6248570]
47. Green H. Cyclic AMP in relation to proliferation of the epidermal cell: a new view. Cell. 1978 Nov. 15:801. [PubMed: 83196]
48. Guo W, et al. Slug and Sox9 cooperatively determine the mammary stem cell state. Cell. 2012 Mar 2.148:1015. [PubMed: 22385965]
49. Daigle SR, et al. Selective killing of mixed lineage leukemia cells by a potent small-molecule DOT1L inhibitor. Cancer cell. 2011 Jul 12.20:53. [PubMed: 21741596]
50. Dong C, et al. G9a interacts with Snail and is critical for Snail-mediated E-cadherin repression in human breast cancer. The Journal of clinical investigation. 2012 Apr.122:1469. [PubMed: 22406531]
51. Dontu G, et al. In vitro propagation and transcriptional profiling of human mammary stem/progenitor cells. Genes & development. 2003 May 15.17:1253. [PubMed: 12756227]
52. Kim D, et al. TopHat2: accurate alignment of transcriptomes in the presence of insertions, deletions and gene fusions. Genome biology. 2013; 14:R36. [PubMed: 23618408]

53. Anders S, Pyl PT, Huber W. HTSeq--a Python framework to work with high-throughput sequencing data. Bioinformatics. 2015 Jan 15.31:166. [PubMed: 25260700]

54. Anders S, Huber W. Differential expression analysis for sequence count data. Genome biology. 2010; 11:R106. [PubMed: 20979621]

55. Langmead B, Salzberg SL. Fast gapped-read alignment with Bowtie 2. Nature methods. 2012 Apr. 9:357. [PubMed: 22388286]

56. Zhang Y, et al. Model-based analysis of ChIP-Seq (MACS). Genome biology. 2008; 9:R137. [PubMed: 18798982]

57. Shin H, Liu T, Manrai AK, Liu XS. CEAS: cis-regulatory element annotation system. Bioinformatics. 2009 Oct 1.25:2605. [PubMed: 19689956]

58. Shen L, Shao N, Liu X, Nestler E. ngs.plot: Quick mining and visualization of next-generation sequencing data by integrating genomic databases. BMC genomics. 2014; 15:284. [PubMed: 24735413]

59. Quinlan AR, Hall IM. BEDTools: a flexible suite of utilities for comparing genomic features. Bioinformatics. 2010 Mar 15.26:841. [PubMed: 20110278]

60. Robinson JT, et al. Integrative genomics viewer. Nature biotechnology. 2011 Jan.29:24.

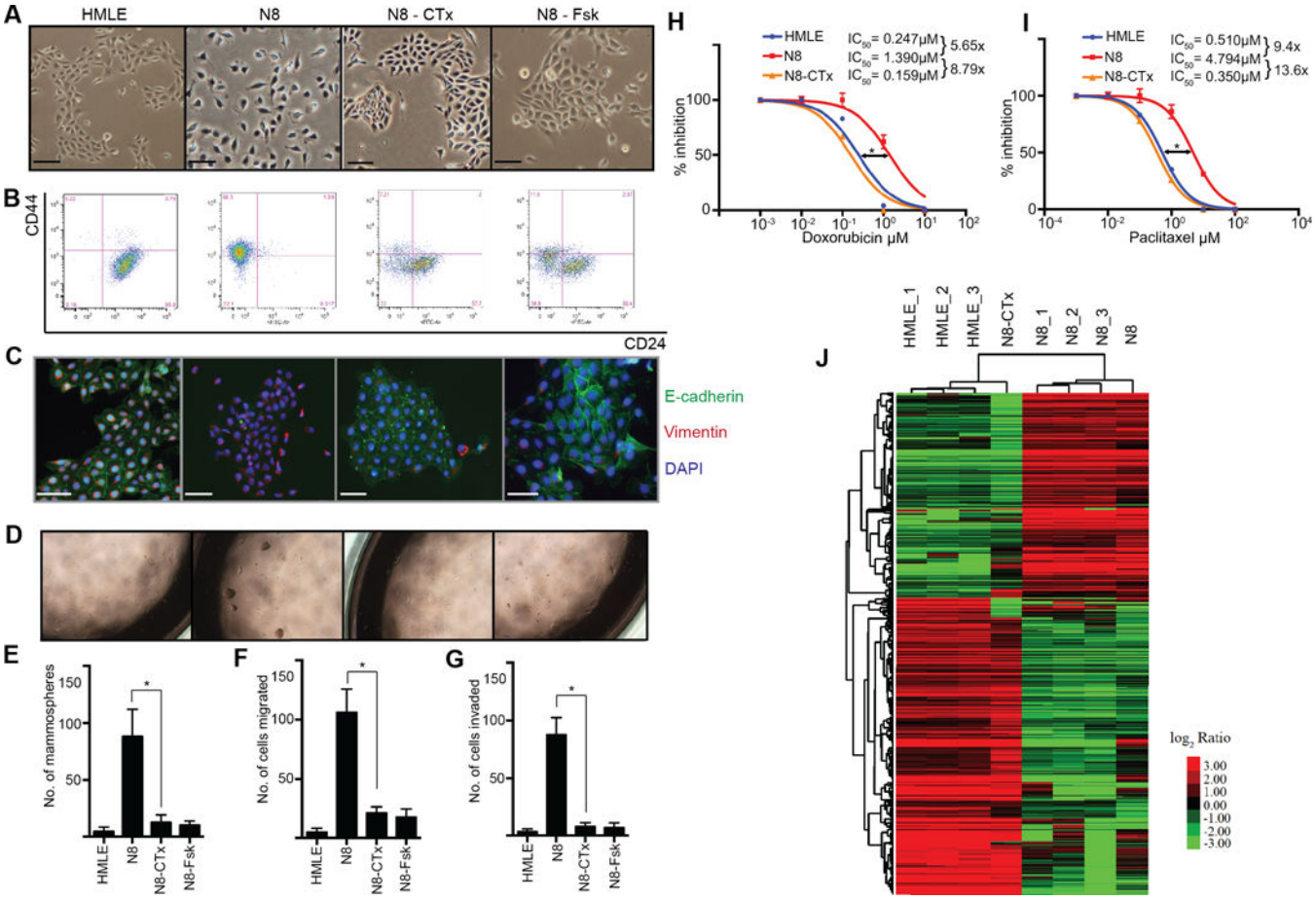

Figure 1. Induction of a mesenchymal-to-epithelial transition (MET) upon treatment of N8 cells with cholera toxin (CTx) or forskolin (Fsk)

Mesenchymal N8 cells acquire an epithelial morphology as adjudged by their morphology (A), loss of a stem-like $CD44^{hi}/CD24^{lo}$ profile to assume a predominantly $CD44^{lo}/CD24^{hi}$ profile (B) and expression of E-cadherin at cell junctions and loss of vimentin (C). Reverted N2-CTx and N3-Fsk cells lose their ability to form (D, E) mammospheres (mean ± SD, $p<0.05$, n=4), (F) migrate (mean ± SD, $p<0.05$, n=4) and (G) invade in transwell assays (mean ± SD, $p<0.05$, n=4) and acquire increased sensitivity to treatment with (H) doxorubicin and (I) paclitaxel (mean ± SD, $p<0.05$, n=4). (J) Heatmap of mRNA-Seq data demonstrating similarity in gene expression between HMLE, N8 and N8-CTx cells. Data in (E), (F) and (G) were analysed by student t-test, (H) and (I) were analysed by Bonferroni correction. All scale bars - 25μm.

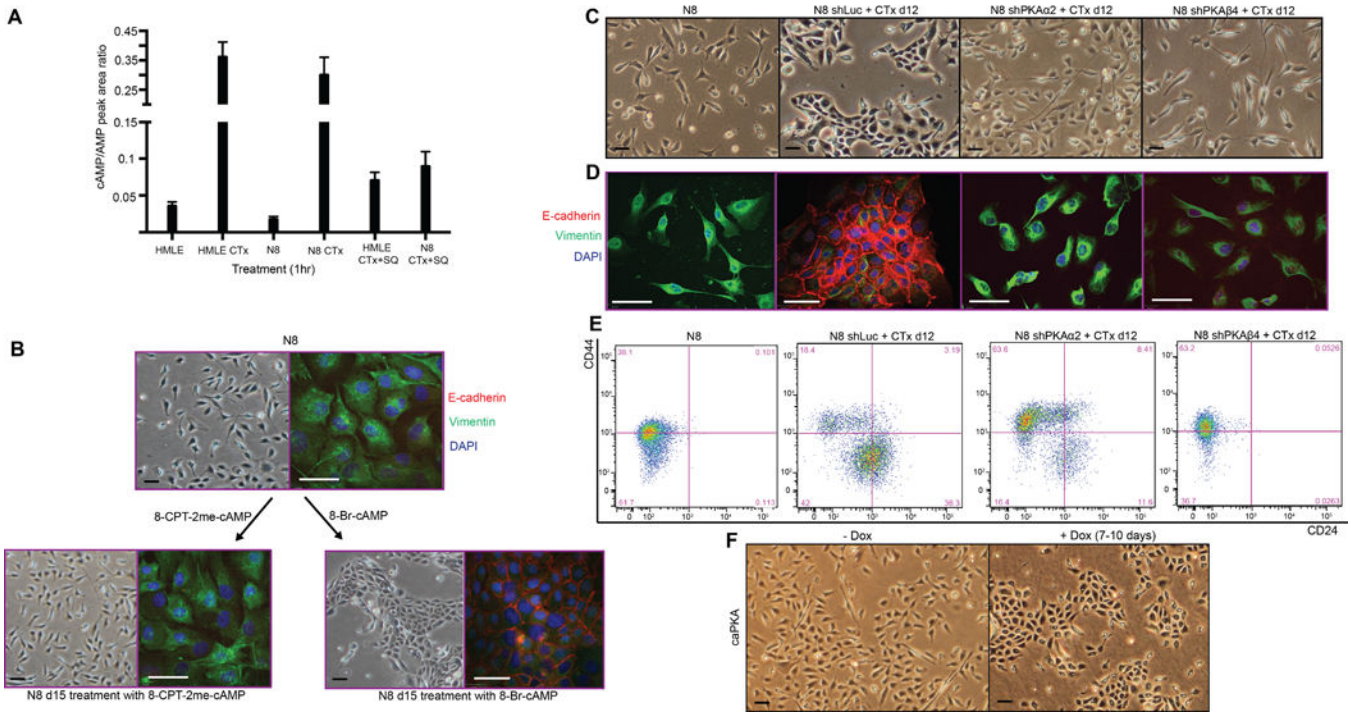

Figure 2. cAMP increases activate protein kinase A (PKA), which is both necessary and sufficient for the induction of an MET in N8 cells

(A) Mass-spectrometry measurement of cAMP levels in N8 cells that have been treated with CTx or Fsk alone and in combination with adenylate cyclase inhibitor SQ (mean ± SD, $p<0.05$, n=3). (B) Treatment of N8 cells with either 8-CPT-2me-cAMP or 8-Br-cAMP to identify downstream pathways that are responsible for induction of an MET. Knockdown of either PRKACA or PRKACB prevents the ability of CTx to induce an MET in N8 cells as observed by changes in (C) morphology, (D) immunofluorescence for E-cadherin and vimentin and (E) CD44/CD24 status. (F) Morphological changes of N8 cells undergoing an MET upon ectopic expression of an active mutant of PKA (caPKA). Data in (A) were analysed using the Student t-test. All scale bars - 25μm.

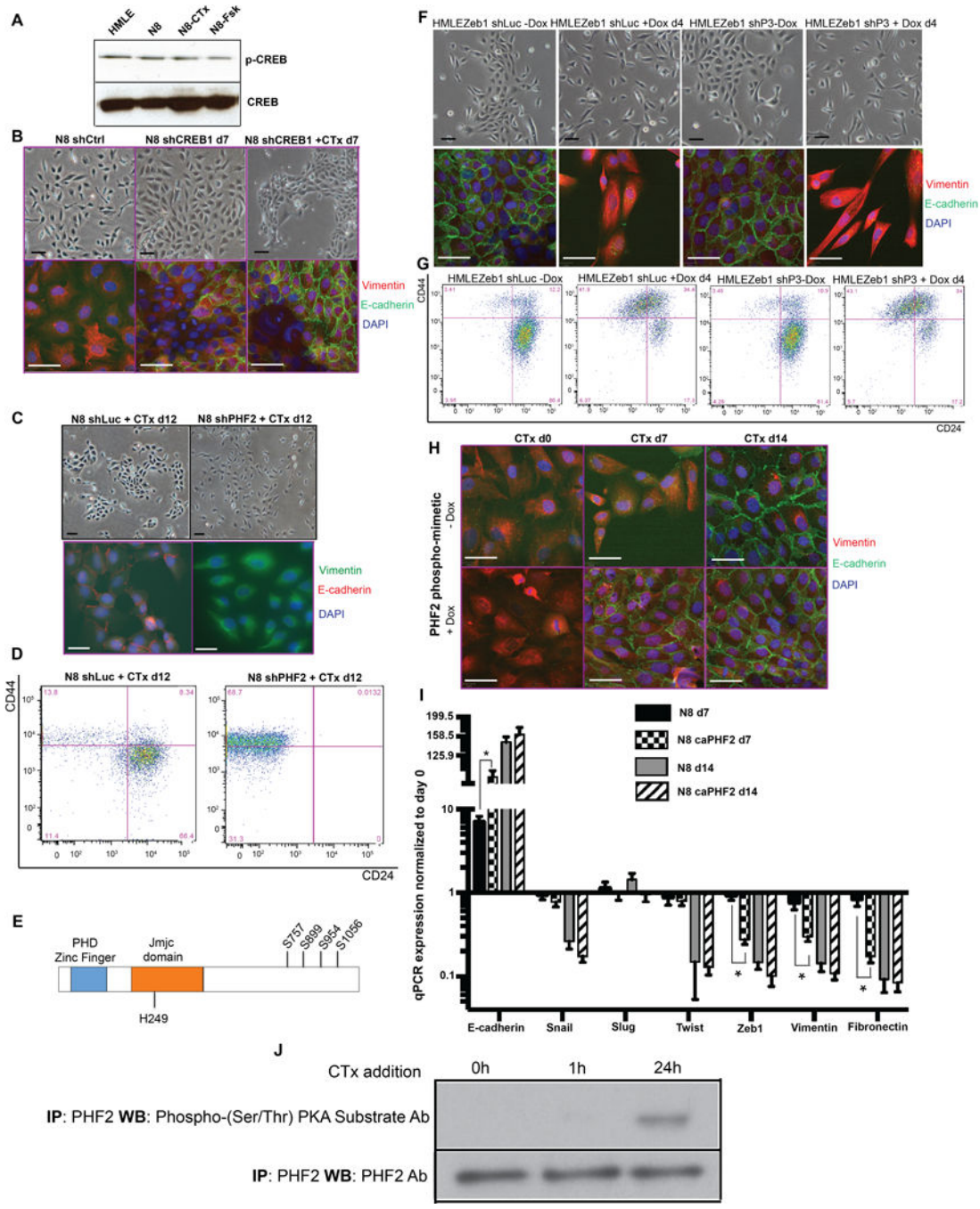

Figure 3. The PKA substrate PHF2, but not CREB1, is necessary for the MET-inducing properties of CTx

Activation state of CREB1 as measured by levels of p-CREB1 across HMLE and N8 cells that have been treated with CTx or Fsk (A). Loss of CREB1 through shRNA-mediated knockdown induces a partial MET and permits CTx-mediated complete MET as shown by changes in morphology and immunofluorescence (B). shRNA-mediated knockdown of PHF2 abrogates the ability of CTx to induce an MET preventing changes in (C) morphology and immunofluorescence-based detection of E-cadherin and fibronectin expression as well as (D) blocking a shift from the $CD44^{hi}/CD24^{lo}$ state to the $CD44^{lo}/CD24^{hi}$ state.

Expression of a PHF2 phosphomimetic where the C-terminal serines were modified to aspartate (E) accelerated the MET transition by 5 days as observed by changes in immunofluorescence (F) and quantitative EMT marker analysis by qPCR (G). Effects of shRNA-mediated knockdown of PHF2 on the ability of HMLE cells to undergo an EMT upon ectopic expression of Zeb1 (H, I) (qPCR data - mean ± SD, $p<0.05$, $n=3$). Immunoprecipitation of PHF2 followed by immunoblotting with a phospho-PKA substrate antibody showing direct phosphorylation of PHF2 by PKA 24hrs after treatment of N8 cells with CTx (J). (I) was analysed using the Student t-test. All scale bars - 25μm.

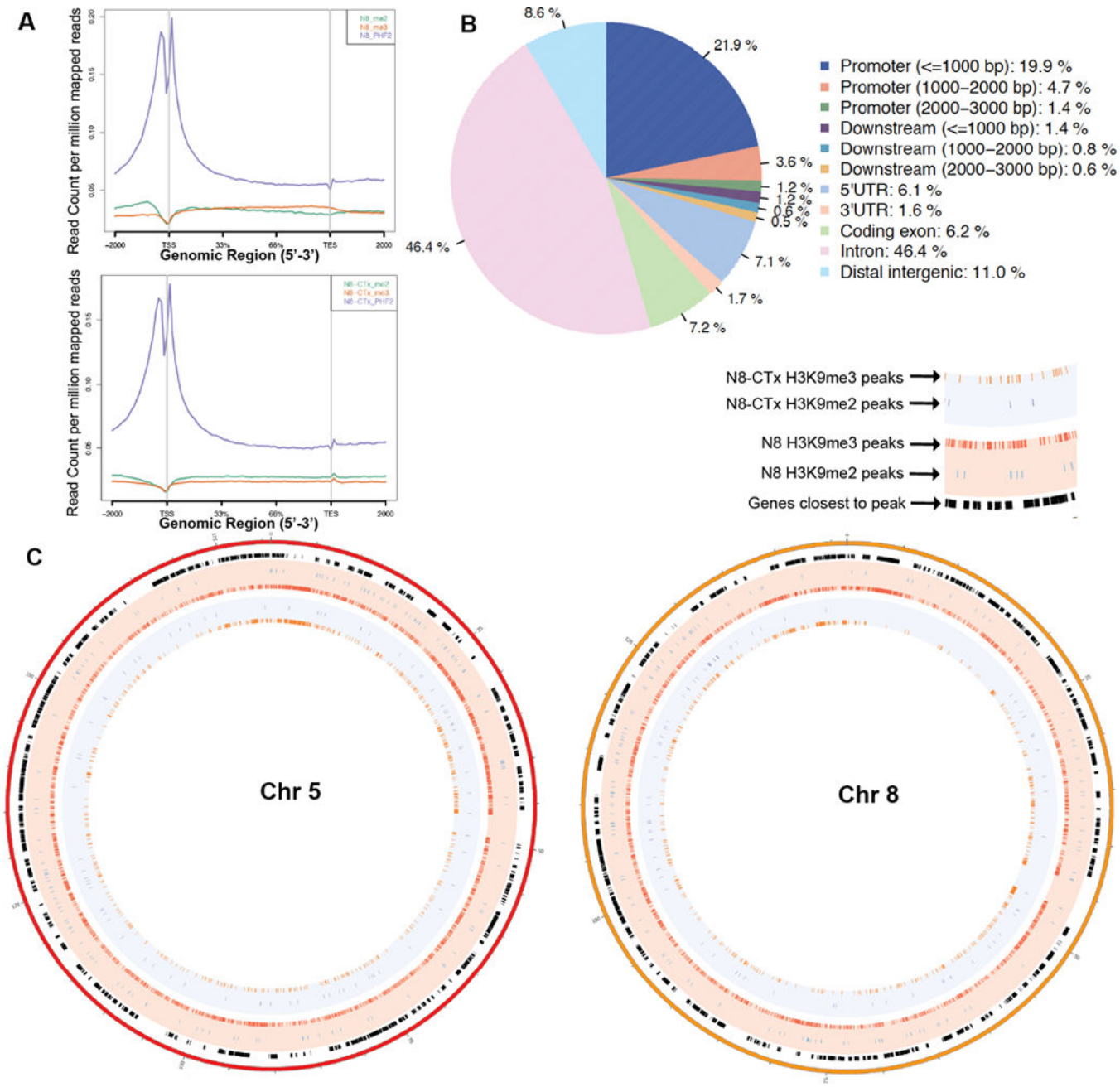

Figure 4. Activation of PHF2 leads the epigenetic reprogramming of mesenchymal cells

Genome-wide occupancy of H3K9me2, H3K9me3 and PHF2 marks shows the inverse correlation between the presence of the histone marks and the demethylase (A), which interacts mainly with the promoter and the first intronic region of genes (B). Circos plots of representative chromosomes 5 and 8 show widespread changes in the H3K9me2 and H3K9me3 profiles (C).

A

Xenograft Line	Cells Transplanted	Tumors	Tumor-initiating frequency
HMLE Ras	2 x 10^6 2 x 10^5 2 x 10^4	10/10 1/10 0/10	1/727615
N8 Ras	2 x 10^6 2 x 10^5 2 x 10^4	10/10 10/10 9/10	1/8686
N8-CTx-Ras	2 x 10^6 2 x 10^5 2 x 10^4	9/10 0/10 0/10	1/1201192

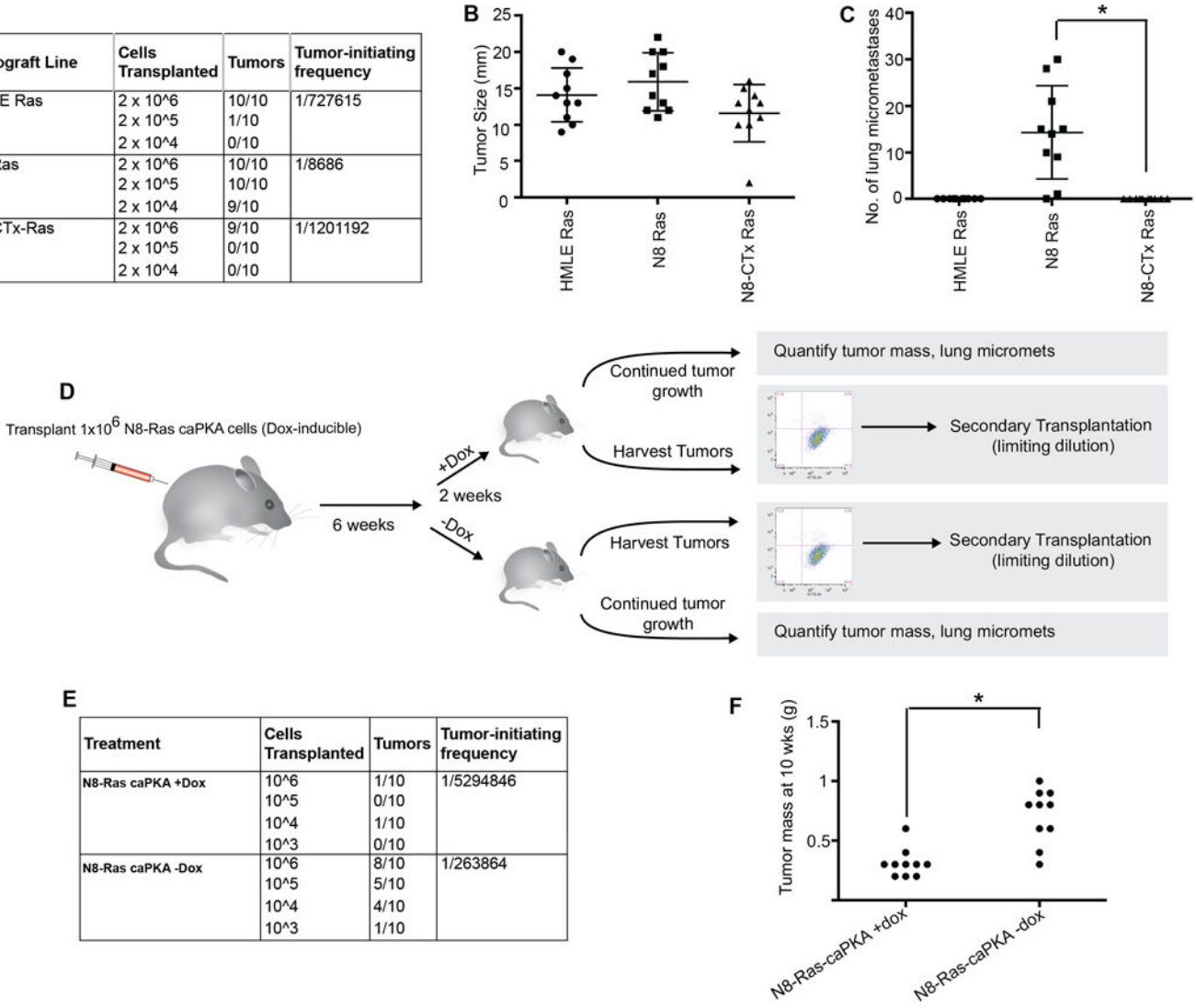

E

Treatment	Cells Transplanted	Tumors	Tumor-initiating frequency
N8-Ras caPKA +Dox	10^6 10^5 10^4 10^3	1/10 0/10 1/10 0/10	1/5294846
N8-Ras caPKA -Dox	10^6 10^5 10^4 10^3	8/10 5/10 4/10 1/10	1/263864

Figure 5. PKA-induced MET is sufficient to deplete the tumor-initiating ability of N8-Ras cells *in vivo*

(A) Table outlining differences in tumor-initiating ability of HMLE-Ras, N8-Ras and N8-CTx-Ras cells upon limiting dilution transplantation into NOD/SCID mice. Tumors that arose from transplantation of 2×10^6 cells were or similar size (B) with only the N8-Ras cells bring capable of forming micrometastases (C) (Each dot represents one mouse; data analysed using Student t-test; $p<0.05$, n=10). (D) Panel showing experimental outline to test the tumor-initiating ability of N8-Ras cells upon transient *in vivo* expression of PKA showing a (E) 20-fold decrease in tumor-initiating ability upon secondary transplantation with (F) no significant differences in the tumor volume. (Each dot represents one mouse; data analysed using Student t-test; $p<0.05$, n=10).